AIP | Applied Physics Letters

Carbon-doped GaAs single junction solar microcells grown in multilayer epitaxial assemblies

Dongseok Kang, Shermin Arab, Stephen B. Cronin, Xiuling Li, John A. Rogers et al.

Citation: Appl. Phys. Lett. **102**, 253902 (2013); doi: 10.1063/1.4812399
View online: http://dx.doi.org/10.1063/1.4812399
View Table of Contents: http://apl.aip.org/resource/1/APPLAB/v102/i25
Published by the AIP Publishing LLC.

Carbon-doped GaAs single junction solar microcells grown in multilayer epitaxial assemblies

Dongseok Kang,[1] Shermin Arab,[2] Stephen B. Cronin,[2] Xiuling Li,[3] John A. Rogers,[3,4] and Jongseung Yoon[1,2,a)]

[1]*Department of Chemical Engineering and Materials Science, University of Southern California, Los Angeles, California 90089, USA*

[2]*Department of Electrical Engineering, University of Southern California, Los Angeles, California 90089, USA*

[3]*Department of Electrical and Computer Engineering, University of Illinois at Urbana-Champaign, Urbana, Illinois 61801, USA*

[4]*Department of Materials Science and Engineering, University of Illinois at Urbana-Champaign, Urbana, Illinois 61801, USA*

(Received 17 May 2013; accepted 2 June 2013; published online 25 June 2013)

A stack design for carbon-doped GaAs single junction solar microcells grown in triple-layer epitaxial assemblies is presented. As-grown materials exhibit improved uniformity of photovoltaic performance compared to zinc-doped systems due to the lack of mobile dopants while a slight degradation exists in middle and bottom devices. Detailed electrical and optical characterizations of devices together with systematic studies of acceptor reactivation reveal carbon-related defects accompanied by carrier compensation, and associated scattering and recombination centers are primarily responsible for the degraded contact properties and photovoltaic performance, resulting from prolonged thermal treatments of early-grown materials during the multilayer epitaxial growth. © *2013 AIP Publishing LLC*. [http://dx.doi.org/10.1063/1.4812399]

III-V compound semiconductors represent enabling materials for a variety of modern technological applications ranging from high-speed electronics, solid-state lighting to energy harvesting.[1–3] In particular, a wide range of accessible band gap energies and other unique features such as excellent radiation hardness and ability to grow ternary or quarternary alloys to tune the band gap and form multiple junctions render these materials exceptionally attractive for realizing ultrahigh efficiency photovoltaic devices.[1,4] Despite their superior materials properties and excellent performance characteristics, application of III-V compound semiconductors in terrestrial photovoltaics has been limited compared to silicon-based systems due to their prohibitively high cost associated with growing device-quality epitaxial materials, but also difficulties in incorporating them over large area, inexpensive substrates.[5] Recently, Yoon *et al*. demonstrated a new concept for the growth and integration of III-V compound semiconductors that can overcome many of these challenges, where multilayer epitaxial assemblies based on GaAs and $Al_xGa_{1-x}As$ were grown on a GaAs substrate such that respective "device layers" can be released in a sequential manner through selective removal of AlAs to generate high quality epitaxial materials in large quantities, thereby leading to significant reduction of materials cost.[6] In previously reported triple-stack GaAs solar cells,[6] however, the photovoltaic performance showed a systematic degradation between device layers grown in different sequences due primarily to mobile p-type dopants, zinc, and resulting modification of materials properties in constituent epitaxial layers. The diffusion of zinc caused a significant deviation from optimized electronic configuration for solar cells, including redistribution of pn-junction profiles as well as carrier compensation in n-type layers.[6] Here, we introduce an alternative stack design for single junction GaAs solar cells grown in multilayer epitaxial assemblies to address adverse effects of mobile impurities by exploiting carbon as p-type dopants. Detailed electrical and optical characterizations of devices together with systematic studies of acceptor reactivation provide some of essential aspects of materials science and physics in carbon-doped GaAs multilayer assemblies for solar cells.

The epitaxial stack for multilayer GaAs solar cells in the present study exploits carbon as p-type dopants to address aforementioned issues of mobile dopants. Zinc is a shallow acceptor that resides on a gallium sub-lattice in GaAs. Due to its order-of-magnitude higher diffusion coefficient, diffusion of zinc takes place on interstitial sites, where the interchange of interstitial (Zn_i^+) and substitutional (Zn_s^-) forms of zinc readily occurs through reactions involving gallium vacancies (V_{Ga}).[7–11] By contrast, carbon predominantly incorporates as substitutional acceptors on the arsenic sub-lattice (C_{As}), resulting in its much lower tendency for diffusion in GaAs compared to zinc even at high doping levels.[12–14] Carbon has been therefore widely used as p-type dopants for GaAs in applications that require a sharp, abrupt dopant profile at high doping concentrations.[15] In carbon-doped GaAs, however, it is often observed that not all carbon atoms are electrically active and the effective hole concentration is substantially lower than the carbon concentration.[16–18] Such electrical passivation of carbon in GaAs is well known to arise from the unintentional incorporation of hydrogen, which spontaneously forms monomeric (C_{As}-H) or dimeric (C_{As}-H-Ga-C_{As}) complexes with carbon to reduce the lattice energy and residual stresses.[17–19] As these hydrogen complexes neutralize electrical activity of the carbon, procedures for reversing hydrogen passivation to recover effective hole concentration are often required for practical application of carbon-doped GaAs, especially for

a)Author to whom correspondence should be addressed. Electronic mail: js.yoon@usc.edu.

devices that demand precise control of doping characteristics. Over the past decades, thermal annealing in inert gas environment has been extensively demonstrated as an effective process to reactivate hydrogen-passivated carbon in GaAs.[19–21] In this study, above-described aspects of carbon as p-type dopants were taken into account in the epitaxial design as well as fabrication steps for carbon-doped multilayer GaAs solar cells. A "p-on-n" device configuration was therefore chosen to facilitate the reactivation process of carbon by exposing p-type layers to the atmosphere for the outdiffusion of hydrogen. A schematic illustration of the stack design appears in Fig. 1(a). Triple-layer stacks of p-on-n GaAs solar cells were grown on a semi-insulating GaAs substrate by metal organic chemical vapor deposition (MOCVD) with sacrificial layers (~500 nm, $Al_{0.95}Ga_{0.05}As$) incorporated between active regions such that respective device layers (i.e., top, middle, and bottom) can be released sequentially from the growth wafer and deposited on foreign substrates (Figs. 1(b) and 1(c)). The semiconductor epitaxial stacks for each device layer are composed of p^+-type GaAs top contact (200 nm, C-doped, $5 \times 10^{18}\,cm^{-3}$), p-type $Al_{0.4}Ga_{0.6}As$ window (40 nm, C-doped, $2 \times 10^{18}\,cm^{-3}$), p-type GaAs emitter (100 nm, C-doped, $2 \times 10^{18}\,cm^{-3}$), n-type GaAs base (2 μm, Si-doped, $3 \times 10^{17}\,cm^{-3}$), n-type $Al_{0.4}Ga_{0.6}As$ back surface field (100 nm, Si-doped, $3.5 \times 10^{18}\,cm^{-3}$), and n^+-type GaAs bottom contact (1.5 μm, Si-doped, 4–5 $\times 10^{18}\,cm^{-3}$), with a total thickness of ~3.94 μm.

We first examined contact properties and photovoltaic performance of GaAs solar cells fabricated from as-grown materials. Microscale solar cells (i.e., microcells) were fabricated using previously reported procedures.[6] Briefly, controlled wet chemical etching of lithographically patterned areas by the mixture of citric acid and hydrogen peroxide defined top and bottom contact regions (~$35 \times 500\,\mu m^2$) and delineated arrays of microcells (~$500 \times 500\,\mu m^2$) on the source wafer, followed by deposition and annealing of n- and p-type contact metals that consist of Pd/Ge/Au (5/35/80 nm) and Pt/Ti/Pt/Au (10/40/10/80 nm), respectively (Fig. 1(c)). Fig. 2(a) shows representative current density (J)-voltage (V) curves of microcells with a single layer antireflection coating (Si_xN_y; $n \sim 2.02$, thickness ~60 nm), measured under simulated AM 1.5G illumination ($1000\,W/m^2$) at room temperature. Corresponding device characteristics of solar cells are summarized in Fig. 2(b). Uniformity of photovoltaic performance in as-grown materials is improved compared to previously reported zinc doped systems[6] due to the lack of mobile dopants, while there exists a small degree of degradation in middle and bottom devices. Average solar-to-electric conversion efficiencies at middle and bottom devices are ~95% and ~91% of the efficiency obtained from the top cells, respectively. Figs. 2(c) and 2(d) show plots of total resistance (R) as a function of contact pad distance (x) for top (p^+-GaAs) and bottom (n^+-GaAs) contact layers, respectively, obtained from standard transmission line model (TLM) measurements.[22] Contact properties for n^+-GaAs including contact (R_c) and sheet resistances (R_s) are in the similar range throughout all device layers as there is no diffusion of p-type dopants and resultant carrier compensation in n-type layers.[6] On the other hand, contact properties for p^+-GaAs showed a noticeable deterioration from top to bottom devices, which is consistent with the

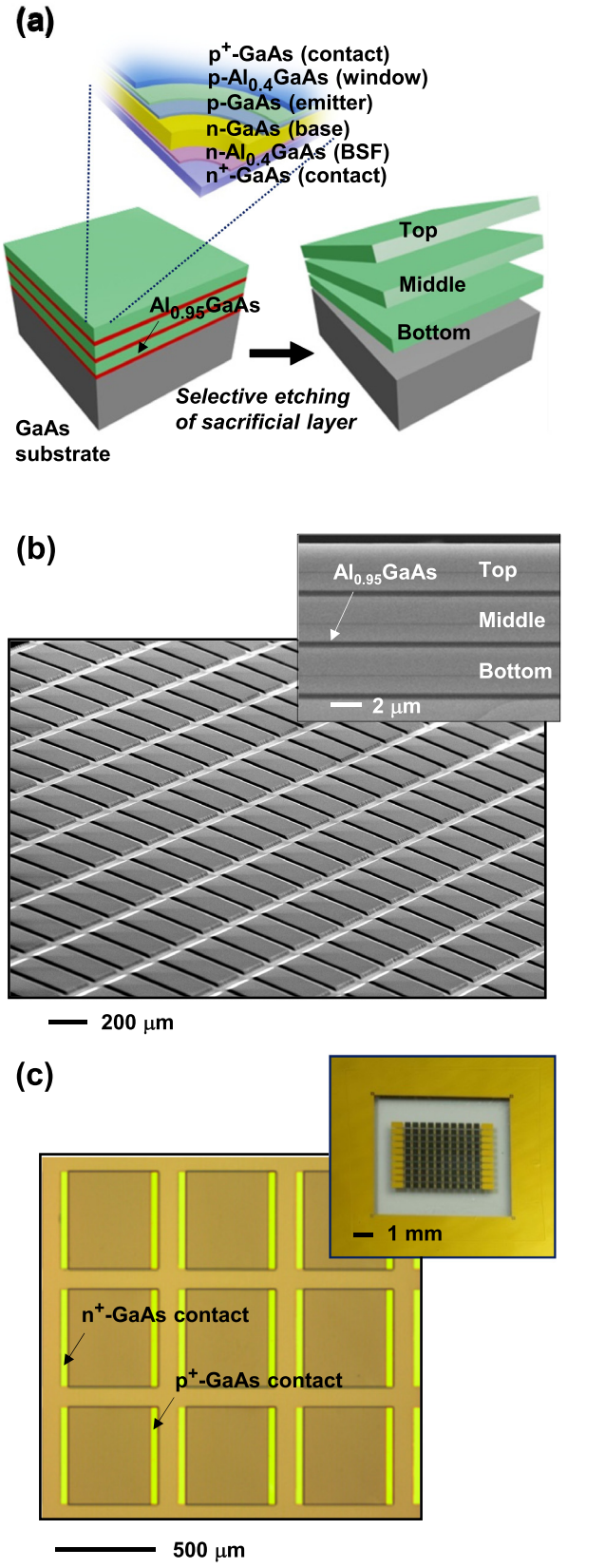

FIG. 1. (a) Schematic illustration and detailed stack configuration of releasable multilayer epitaxial assemblies of p-on-n type single junction GaAs solar cells grown on a GaAs substrate by MOCVD. (b) Tilt-view SEM image of isolated arrays of triple-stack GaAs solar cells. Inset: cross-sectional view of the stack, where thick, dark regions correspond to the sacrificial layer ($Al_{0.95}Ga_{0.05}As$) separating respective device layers. (c) Photographic image of isolated arrays of completed GaAs solar cells on a source wafer. Inset: optical image of completed microcells printed and interconnected on a polyethylene terephthalate (PET) substrate.

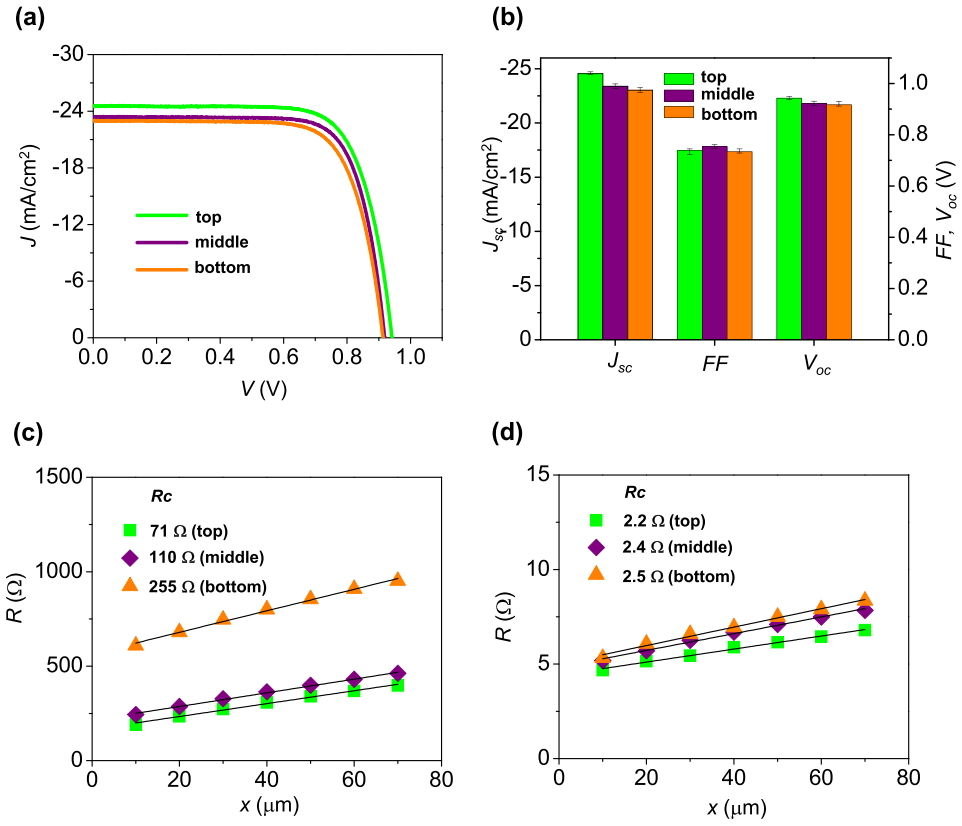

FIG. 2. (a) Representative current density (J)-voltage (V) curves of as-grown, carbon-doped GaAs solar cells formed from top, middle, and bottom device layers, measured under AM 1.5G illumination on the source wafer. (b) Corresponding short-circuit current density (J_{sc}), fill factor (FF), and open circuit voltage (V_{oc}) extracted from JV characteristics of solar cells in (a). Error bars indicate maximum and minimum values. (c) Plot of total resistance (R) as a function of metal pad spacing (x) from standard TLM measurements for p^+-GaAs contacts (Pt/Ti/Pt/Au) at top, middle, and bottom devices of as-grown materials, where thermal annealing was conducted before the measurement at 400 °C for 1 min under 100% N_2 atmosphere. Contact resistance (R_c) was obtained from one half of the y-intercept in the linear fit of data. (d) Plot of R vs. x for n^+-GaAs contacts (Pd/Ge/Au) at top, middle, and bottom devices of as-grown materials. Ohmic contacts were formed by thermal annealing at 175 °C for 1 h under 100% N_2 atmosphere.

degradation of photovoltaic performance but also indicates that there is a progressive reduction of effective hole concentrations or carrier mobility in middle and bottom devices.

Secondary ion mass spectrometry (SIMS) and low temperature photoluminescence measurements in as-grown materials were carried out to examine the origin of degraded contact properties and photovoltaic performance. SIMS depth profiles for p-type layers in top, middle, and bottom devices are shown in Figs. 3(a)–3(c), where green and purple lines are atomic concentrations (in atoms per cm^3) of carbon and hydrogen, respectively. The orange data points are the intensity of secondary ions from aluminum, where the peak corresponds to the p-type $Al_{0.4}Ga_{0.6}As$ window layer. The carbon concentration in p^+-contact layers was comparable in top and middle

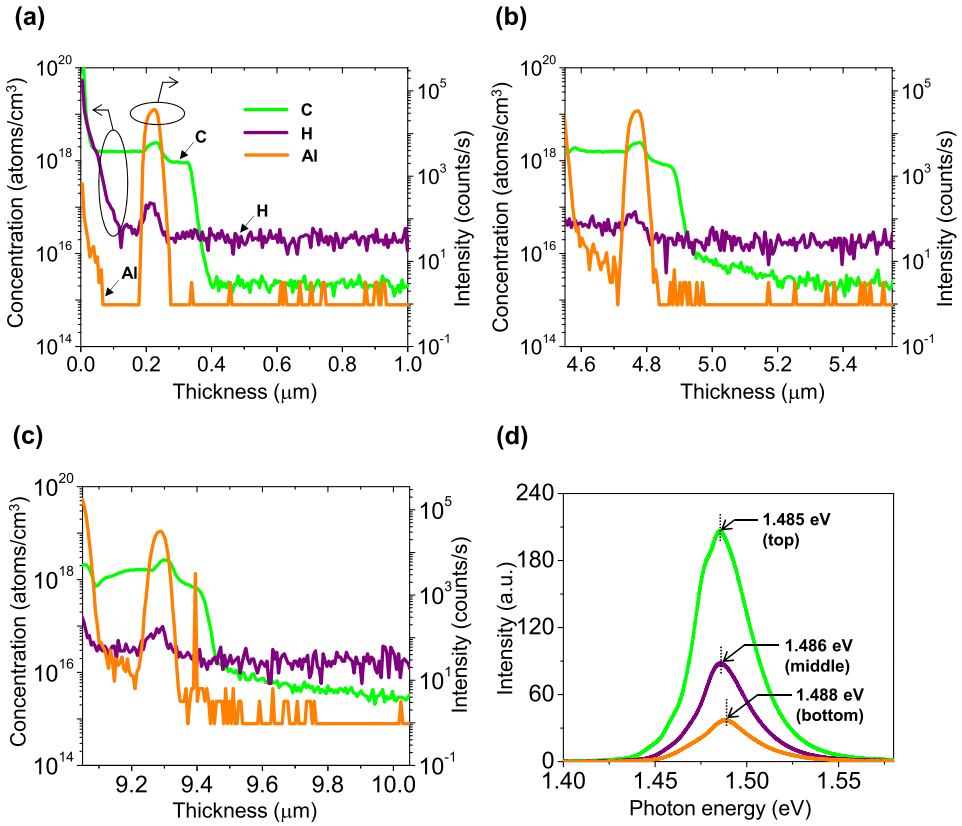

FIG. 3. Atomic concentration profiles of carbon (green line) and hydrogen (purple line) with as-grown triple-stack GaAs solar cells obtained from SIMS, where regions near p-type layers are highlighted for (a) top, (b) middle, and (c) bottom devices, respectively. The orange data points are the intensity of secondary ions from aluminum, where the peak corresponds to the window layer ($Al_{0.4}Ga_{0.6}As$). (d) Low temperature photoluminescence spectra for as-grown top, middle, and bottom GaAs solar cells measured at 77 K, where a 532 nm laser was used as an excitation source illuminated at the exposed surface of p^+-GaAs contact layer.

devices, while it was slightly lower in bottom devices. The hydrogen concentration in p-type layers was relatively uniform in all devices and much lower than the carbon concentration, which suggests that the level of hydrogen passivation is not as severe as expected from the degraded contact properties. Additionally, low temperature photoluminescence (PL) measurement was performed at 77 K on each device layer as summarized in Fig. 3(d). A 532 nm laser (~0.05 mW) was used as an excitation light source on the exposed surface of p^+-GaAs contact layer, where the peaks near 1.485 eV correspond to transitions from conduction band to acceptor levels.[23,24] The PL spectra evidently showed that the intensity of peaks substantially decreased from top to bottom devices. This indicates that epitaxial quality of carbon-doped layers in middle and bottom devices is significantly different from top devices, which might be attributed to carbon-related defects or crystal imperfections that can act as nonradiative recombination centers.[25] It was also observed that the peak position of PL spectra shifted in small degrees to the lower energy, which also agrees with the trend of decrease in effective hole concentrations.[26]

In order to further assess the effect of acceptor passivation on observed nonuniform contact properties and photovoltaic performance, *ex situ* thermal annealing was conducted under 100% nitrogen atmosphere at 450 °C, which involves multi-step processes such as dissociation of hydrogen from carbon-hydrogen complexes, its out-diffusion to the atmosphere, and recovery of shallow acceptor levels.[18,19,21] In the present study, the effectiveness of carbon reactivation was evaluated by monitoring changes of contact properties in p^+-GaAs layers obtained from standard TLM measurements before and after thermal annealing, where contact properties of as-grown materials served as a reference. Samples of top, middle, and bottom devices with exposed p^+-GaAs contact layers were annealed at 450 °C for two different time periods (that is, 20 and 40 min) under 100% nitrogen atmosphere before contact metals were deposited. Figs. 4(a)–4(c) illustrate percentage changes of contact resistance ($(R_c - R_{c0})/R_{c0} \times 100$) and sheet resistance ($(R_s - R_{s0})/R_{s0} \times 100$), compared to as-grown materials, where R_{c0} (R_{s0}) and R_c (R_s) correspond to contact resistance (sheet resistance) of as-grown and reactivated materials, respectively. Thermal annealing at 450 °C improved contact properties for all device layers compared to as-grown materials due to the effect of hydrogen out-diffusion, while their detailed characteristics such as the level of improvement and activation kinetics were distinctively different. For the top devices, annealing for 40 min showed comparatively larger improvement than 20 min, while the effectiveness of 40 min annealing was similar to, or slightly worse than 20 min in middle and bottom devices, respectively. Such variation of reactivation behaviors under the same annealing condition suggests that the nature of acceptor passivation such as types of carbon-hydrogen complexes and their composition might be different between respective devices in as-grown materials. In particular, dimeric carbon-hydrogen complexes are known to exhibit slower dissociation kinetics than monomeric forms at a given annealing temperature and introduce deep acceptor levels that can serve as active recombination centers.[19,21] They also do not contribute to the increase of effective hole concentration even after the release of hydrogen.[19,21] In connection to the observation that carbon concentrations of top and middle devices are about the same as shown in SIMS profiles (Figs. 3(a) and 3(b)), the shorter reactivation time in middle devices could be explained by their comparatively higher concentration of dimeric carbon-hydrogen complexes. It is also notable that contact properties (i.e., R_c and R_s) in middle and bottom devices did not fully recover to the level of top devices even after the reactivation processes. This result is consistent with the SIMS data that

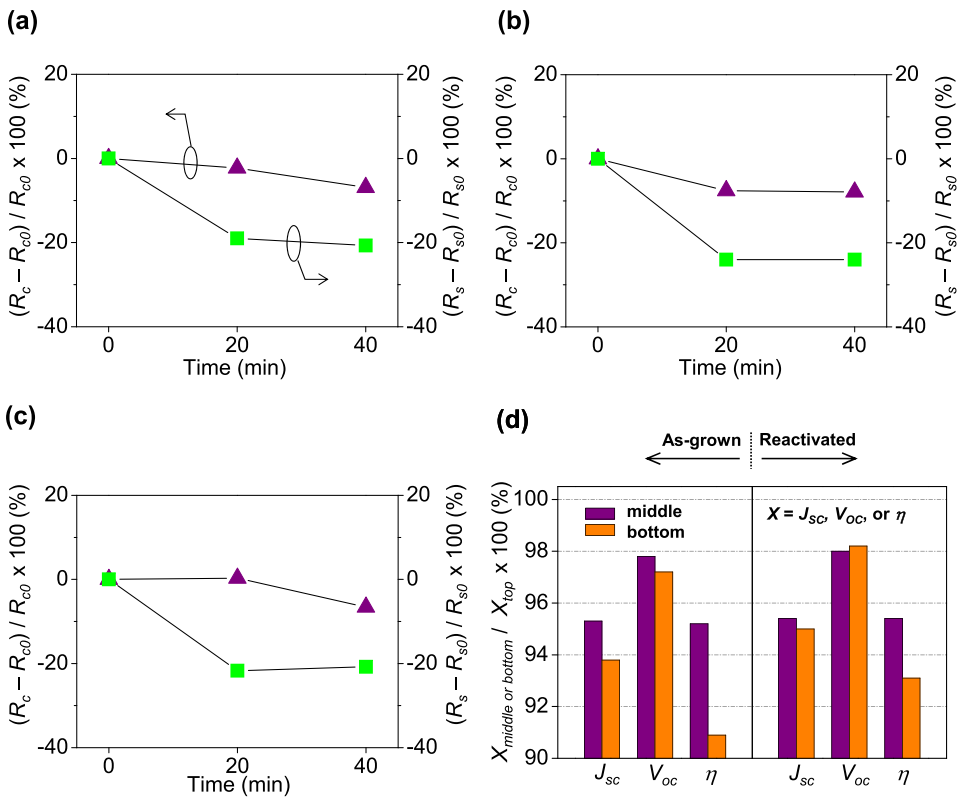

FIG. 4. Percentage changes of contact resistance ($(R_c - R_{c0})/R_{c0} \times 100$, purple triangle) and sheet resistance ($(R_s - R_{s0})/R_{s0} \times 100$, green square) compared to as-grown materials as a function of annealing time for (a) top, (b) middle, and (c) bottom devices, respectively, where R_{c0} (R_{s0}) and R_c (R_s) correspond to contact resistance (sheet resistance) of as-grown and reactivated materials obtained from standard TLM measurements. (d) Comparison of key device characteristics such as short circuit current density (J_{sc}), open circuit voltage (V_{oc}), and solar energy conversion efficiency (η) between as-grown (left-hand side) and reactivated (right-hand side) materials for middle and bottom devices, where properties in as-grown top devices served as a baseline (i.e., 100%).

indicate low degrees of hydrogen passivation, suggesting there exist additional processes responsible for the degradation of electrical and optical properties in p-type layers. Possible mechanisms that may explain the observation include carbon donors occupying gallium sublattice (C_{Ga}),[27–29] carbon interstitials (C_i),[28,30] or donor-like GaAs point defects such as As antisites,[27,28] which are known to form spontaneously under high temperature annealing. In the multilayer epitaxial growth where middle and bottom device layers have to undergo an extended period of thermal treatments, such carbon-related defects can play an important role in carrier compensation but also further deteriorating materials qualities by generation of scattering and recombination centers. Based on evaluations of contact properties after the thermal annealing, reactivation of p-type epitaxial layers in microcells was also carried out using annealing conditions that provided the largest improvement in each device layer (Figs. 4(a)–4(c)), followed by measurements of photovoltaic device characteristics to evaluate the effect of acceptor reactivation on overall device performance. Fig. 4(d) summarizes the results, where percentage changes of key device characteristics such as short circuit current density (J_{sc}), open circuit voltage (V_{oc}), and solar energy conversion efficiency (η) after the acceptor reactivation, where the performance of as-grown top devices served as a baseline for comparison. The partial recovery of effective hole concentration after the acceptor reactivation translated to a finite enhancement of η both in middle and bottom devices, where V_{oc} slightly improved due to the increase of effective hole concentration in p-type contact and emitter layers. This limited effect of acceptor reactivation upon solar cell characteristics also supports that deteriorated materials properties accompanied by reduction of effective hole concentrations are primarily responsible for the degraded contact properties and photovoltaic device performance. We postulate such degradation of epitaxial quality likely results from prolonged thermal treatments during the multilayer epitaxial growth and might be associated with carbon donors or other carbon-related defects such as carbon interstitials and carbon-hydrogen complexes, all of which contribute to the compensation of holes but also can lead to the increase of scattering and recombination centers that are detrimental for minority carrier transport and therefore solar cell performance. Clearly, further studies will be required for more accurate identification of carbon-related defects and clarification of exact mechanisms for materials deterioration in multilayer epitaxial growth.

To summarize, epitaxial design, materials, and device characteristics of carbon-doped multilayer GaAs solar cells have been presented. Due to the lack of mobile dopants, photovoltaic performance in as-grown materials exhibits improved uniformity compared to zinc doped systems. A small degree of performance degradation in middle and bottom devices is primarily attributed to deteriorated materials properties including carrier compensation, carbon-related defects, and associated scattering and recombination centers, which might result from prolonged thermal treatments of early-grown materials during the multilayer epitaxial growth. Careful control over the growth parameters and annealing conditions to minimize or eliminate such dopant-related defects and crystal imperfections therefore represents an important next step for practical application of multilayer epitaxial assemblies in advanced photovoltaics and optoelectronics, where we expect the results presented here serve as a foundation for future studies.

D. Kang and J. Yoon gratefully acknowledge support from DARPA YFA program under Award No. N66001-12-1-4244 and a start-up grant from the University of Southern California. S. Cronin and S. Arab acknowledge support from the Center for Energy Nanoscience (CEN), an Energy Frontier Research Center (EFRC) funded by the U.S. Department of Energy, Office of Science and Office of Basic Energy Sciences, under Award No. DE-SC0001013. Authors thank Dr. Chia-Chi Chang and Dr. Sung-Min Lee for help on PL measurements and schematics, respectively.

[1]J. F. Geisz and D. J. Friedman, Semicond. Sci. Technol. **17**(8), 769 (2002).
[2]M. R. Krames, O. B. Shchekin, R. Mueller-Mach, G. O. Mueller, L. Zhou, G. Harbers, and M. G. Craford, J. Disp. Technol. **3**(2), 160 (2007).
[3]M. Heyns and W. Tsai, MRS Bull. **34**(7), 485 (2009).
[4]A. Goetzberger, C. Hebling, and H. W. Schock, Mater. Sci. Eng. R **40**(1), 1 (2003).
[5]A. Luque and S. Hegedus, *Handbook of Photovoltaic Science and Engineering* (John Wiley & Sons, Ltd., 2003).
[6]J. Yoon, S. Jo, I. S. Chun, I. Jung, H. S. Kim, M. Meitl, E. Menard, X. L. Li, J. J. Coleman, U. Paik, and J. A. Rogers, Nature (London) **465**(7296), 329 (2010).
[7]L. R. Weisberg and J. Blanc, Phys. Rev. **131**(4), 1548 (1963).
[8]B. Tuck and M. A. H. Kadhim, J. Mater. Sci. **7**(5), 585 (1972).
[9]P. M. Enquist, J. Cryst. Growth **93**(1–4), 637 (1988).
[10]A. H. van Ommen, J. Appl. Phys. **54**(9), 5055 (1983).
[11]G. Rajeswaran, K. B. Kahen, and D. J. Lawrence, J. Appl. Phys. **69**(3), 1359 (1991).
[12]B. T. Cunningham, L. J. Guido, J. E. Baker, J. S. Major, N. Holonyak, and G. E. Stillman, Appl. Phys. Lett. **55**(7), 687 (1989).
[13]L. W. Yang, P. D. Wright, V. Eu, Z. H. Lu, and A. Majerfeld, J. Appl. Phys. **72**(5), 2063 (1992).
[14]B. T. Cunningham, M. A. Haase, M. J. McCollum, J. E. Baker, and G. E. Stillman, Appl. Phys. Lett. **54**(19), 1905 (1989).
[15]S. Gotoh, T. Ueda, H. Kakinuma, and M. Akiyama, Sol. Energy Mater. Sol. Cells **50**(1–4), 281 (1998).
[16]I. Szafranek and G. E. Stillman, J. Appl. Phys. **68**(7), 3554 (1990).
[17]R. Rahbi, B. Pajot, J. Chevallier, A. Marbeuf, R. C. Logan, and M. Gavand, J. Appl. Phys. **73**(4), 1723 (1993).
[18]S. A. Stockman, A. W. Hanson, S. M. Lichtenthal, M. T. Fresina, G. E. Hofler, K. C. Hsieh, and G. E. Stillman, J. Electron. Mater. **21**(12), 1111 (1992).
[19]J. Mimila-Arroyo, A. Lusson, J. Chevallier, M. Barbe, B. Theys, F. Jomard, and S. W. Bland, Appl. Phys. Lett. **79**(19), 3095 (2001).
[20]Q. J. Hartmann, H. Hwangbo, A. Yung, D. A. Ahmari, M. T. Fresina, J. E. Baker, and G. E. Stillman, Appl. Phys. Lett. **68**(7), 982 (1996).
[21]J. Mimila-Arroyo, S. Bland, and M. Barbe, J. Appl. Phys. **91**(9), 5923 (2002).
[22]G. K. Reeves and H. B. Harrison, Electron Device Lett. **3**(5), 111 (1982).
[23]L. Wang, N. M. Haegel, and J. R. Lowney, Phys. Rev. B **49**(16), 10976 (1994).
[24]N. Pan, S. S. Bose, M. H. Kim, G. E. Stillman, F. Chambers, G. Devane, C. R. Ito, and M. Feng, Appl. Phys. Lett. **51**(8), 596 (1987).
[25]H. Fushimi and K. Wada, J. Appl. Phys. **82**(3), 1208 (1997).
[26]S. I. Kim, M. S. Kim, Y. Kim, K. S. Eom, S. K. Min, and C. Lee, J. Appl. Phys. **73**(9), 4703 (1993).
[27]K. Watanabe and H. Yamazaki, Appl. Phys. Lett. **59**(4), 434 (1991).
[28]T. J. Delyon, J. M. Woodall, M. S. Goorsky, and P. D. Kirchner, Appl. Phys. Lett. **56**(11), 1040 (1990).
[29]C. R. Abernathy, S. J. Pearton, R. Caruso, F. Ren, and J. Kovalchik, Appl. Phys. Lett. **55**(17), 1750 (1989).
[30]G. E. Hofler and K. C. Hsieh, Appl. Phys. Lett. **61**(3), 327 (1992).